DOI: 10.1088/1361-6668/acdf8c
FERMILAB-PUB-23-099-TD
(accepted)

Significant reduction in the low-field magnetization of Nb_3Sn superconducting strands using the internal oxidation APC approach

X Xu[1], M Sumption[2], F Wan[1], X Peng[3], J Rochester[2], and E S Choi[4]

[1] Fermi National Accelerator Laboratory, Batavia, IL 60510, U.S.A

[2] The Ohio State University, Columbus, OH 43210, U.S.A

[3] Hyper Tech Research Incorporated, 539 Industrial Mile Road, Columbus, OH 43228, U.S.A

[4] National High Magnetic Field Laboratory, Florida State University, Tallahassee, FL 32310, U.S.A

E-mail: xxu@fnal.gov

Abstract

Nb_3Sn superconductors are promising for building accelerator magnets for future energy-frontier circular colliders. A critical factor for this application is the low-field persistent-current magnetization because it leads to several critical issues: e.g., low-field instability (including flux jumps), hysteresis loss, and field errors in magnet bores. Suppression of low-field magnetization requires reduction of low-field critical current density (J_c) or effective subelement size (d_{eff}). However, reduction of d_{eff} of state-of-the-art Nb_3Sn conductors – the restacked-rod-process (RRP®) type – below 40-50 μm without a pronounced decrease in high-field J_c is difficult. On the other hand, the internal oxidation method which forms artificial pinning centers (APC) in Nb_3Sn offers an alternative approach to reducing the low-field magnetization. Compared with a conventional Nb_3Sn conductor whose flux pinning force versus field (F_p-B) curve peaks at ~20% of its irreversibility field (B_{irr}), the F_p-B curve peaks of APC conductors shift to higher fields due to the point pinning effect, leading to flattening of the J_c-B curves. The goal of this paper is to

quantitatively study how much the APC approach can reduce the low-field magnetization. We measured the J_c-B curves of an RRP® conductor and two APC conductors (reacted at 700°C) from zero field to B_{irr} using a high-field vibrating sample magnetometer (VSM). The results showed that the APC conductors have higher non-Cu J_c at high fields (e.g., 32-41% higher at 16 T) and simultaneously lower non-Cu J_c at low fields (e.g., 28-34% lower at 1 T) compared with the RRP®. This effect is due to a competition between their Nb_3Sn layer fraction ratios and layer F_p ratios. Suppose they reach the same 16 T non-Cu J_c, then the 1 T non-Cu J_c and magnetization of the APC conductors are only half or even less compared with the RRP® conductor.

Keywords: Nb_3Sn Superconductor, Artificial pinning center, Internal oxidation, Magnetization.

1. Introduction

Nb_3Sn is one of the most promising superconductors for building accelerator magnets for future energy-frontier circular colliders – such as hadron colliders [1] or muon colliders [2]. For this application Nb_3Sn dipoles can provide fields up to 16-17 T, while higher fields require high temperature superconductors (HTS), most likely as part of Nb_3Sn/HTS hybrid magnets [3]. However, the performance of current state-of-the-art Nb_3Sn conductors is not sufficient for building cost-effective 16 T dipoles. A comprehensive overview of the R&D needs for Nb_3Sn conductors for high energy physics applications is given in [4], in which three major challenges for present Nb_3Sn conductors are identified. The first challenge is the critical current density (J_c). In order to build efficient coils operating at 16 T, a specification on conductor non-Cu J_c (here

denoted $J_{c,non\text{-}Cu}$), which is at least 1500 A/mm^2 at 4.2 K and 16 T, was determined based on the optimal coil current density [4,5]. Even the best commercial Nb_3Sn conductors presently, which are the restacked-rod-process (RRP®) type, still need significant improvement in order to meet this specification [4,5]. Thus, in recent years the major focus in the community for Nb_3Sn conductor development has been on $J_{c,non\text{-}Cu}$ improvement. The second and third challenges for present Nb_3Sn conductors identified in [4] are the low-field magnetization and the conductor cost, while other challenges, such as the performance degradation under stress and strain, are also critical for high-field applications.

Regarding the second challenge mentioned above, the persistent-current magnetization (M) is proportional to the product of conductor J_c and effective subelement size (d_{eff}). The magnetization of Nb_3Sn conductors may still be acceptable for the high-luminosity upgrade of the large hadron collider (HL-LHC) project, but it is a serious concern for future circular colliders because of the much higher $J_{c,non\text{-}Cu}$ required and the large number of magnets involved [1,4]. So far the magnetization issue has received little attention in the Nb_3Sn conductor community, but in fact M has critical influences on accelerator magnets because it can cause several problems: the low-field instability (including flux jumps), the hysteresis loss, and the field errors in the magnet bores. The three problems are briefly discussed below.

(1) Low-field instability. Magnetization is the driving force for flux jumps [6,7]. Higher M leads to more severe flux jumps (wider flux jump regions and larger amplitude [8]). The flux jumps may not only lead to conductor premature quenches, but also make the correction of the field errors in the magnet bores difficult.

(2) Alternating current (AC) loss. Persistent-current magnetization of superconductors also leads to AC loss [6], which equals to an integration of the magnetization over a field range. As the required conductor $J_{c,non\text{-}Cu}$ is higher and the field range for a full magnet cycle is larger (e.g., from 1 to 16 T and back to 1 T), the AC loss has become more of a concern for accelerator magnets of future circular colliders [1]. A calculation in [9] shows that for the designed 16 T dipoles, the persistent-current M is the major contributor to the AC loss, which is much larger than the goal of 5 kJ/m for the magnets. This will add a significant heat load to the cryogenic plants and the operational cost of the accelerators.

(3) Field errors. Accelerator magnets have demanding requirements on the quality of the fields. The persistent-current magnetization of superconductors is one of the most important factors determining the field errors in the magnet bores [10,11]. In particular, the field errors must be below a certain limit at the injection field of an accelerator magnet cycle. For the 16 T dipoles for future circular colliders, the injection field will most likely be around 1 T [1,4]. In order to limit the field errors at this injection field, a requirement on the magnetization was proposed in [4], with the $\mu_0\Delta M$ (the height of the magnetization versus field loop) at 1 T below 150 mT (normalized to the whole-strand volume). The $\mu_0\Delta M$(1 T) of present state-of-the-art Nb_3Sn conductors is much larger than this requirement (to be shown later) despite their lower $J_{c,non\text{-}Cu}$ than the above-mentioned 16 T $J_{c,non\text{-}Cu}$ specification. It is pointed out in [4] that the field errors generated by the magnetization of the high-$J_{c,non\text{-}Cu}$ Nb_3Sn conductors and the associated flux jumps are too large to allow for sufficient correction.

Overall, the three issues all required a significant reduction of M. In order to reduce M to an acceptable level for the field errors, a goal of conductor d_{eff} of 20 μm was proposed in [4]. However, whether this d_{eff} goal is achievable is a question. Previous measurements showed that

for RRP® strands d_{eff} is generally larger than the physical subelement size, d_{sub} [12-14] – e.g., the results in [12,13] showed that d_{eff} is about 30% larger than d_{sub}. In contrast, for powder-in-tube (PIT) strands d_{eff} is generally much closer to d_{sub} [14]. This is mainly because the unreacted Nb fraction is only 5-10% in RRP® subelements but about 25% in PIT subelements (filaments). In the past two decades there have been significant efforts in reducing the d_{sub} for RRP® strands, enabling a decrease of d_{sub} to 35 μm [13,15]. However, further reducing d_{sub} below 35 μm is difficult because $J_{c,non\text{-}Cu}$ drops quickly as the d_{sub} is below 35-40 μm [15,16] (corresponding to a d_{eff} of nearly 50 μm based on the discussions above). On the other hand, achieving small d_{sub} is easier for PIT and tube type Nb_3Sn conductors, because each of their subelements is just one filament (in comparison, each RRP® subelement is composed of hundreds of Nb filaments, with each filament jacketed by an ultrathin Cu layer). High-filament-count PIT and tube type conductors with d_{sub} as small as 25 μm and 12-16 μm, respectively, have been demonstrated, but the $J_{c,non\text{-}Cu}$ values were far below the above-mentioned $J_{c,non\text{-}Cu}$ specification [17-19]. Similar to the RRP®-type, PIT and tube type conductors also see $J_{c,non\text{-}Cu}$ drop with decreasing d_{sub} (although to a less severe extent), perhaps mainly due to a higher occurrence of filaments with degraded quality (e.g., those with distorted shapes or eccentric cores that can cause early Sn leakage before a full Nb_3Sn layer is grown). Overall, it seems that reducing d_{eff} to 20 μm is not realistic for RRP® strands, and is also very difficult for PIT and tube type strands if we want to achieve high $J_{c,non\text{-}Cu}$ at the same time.

On the other hand, a new type of Nb_3Sn conductor, which contains artificial pinning centers (APC) formed via the internal oxidation method, offers an alternative approach to reducing the low-field M. From the above discussions we can see that it is the M at low fields that is the major concern, because the M at low fields (e.g., 1-3 T) is many times larger than that at high fields

(e.g., above 12 T). Our original purpose for developing the APC Nb_3Sn strands was to enhance the high-field J_c [20,21], because the internal oxidation forms oxide particles (with diameters mostly below 10 nm [22]), which not only significantly refine Nb_3Sn grain size, but also serve as point pinning centers themselves, both effects leading to higher flux pinning force (F_p) and thus higher J_c at high fields [23]. The $J_{c,non\text{-}Cu}$ of our APC strands has not only surpassed the state-of-the-art Nb_3Sn conductors, but also surpassed the above-mentioned 16 T $J_{c,non\text{-}Cu}$ specification [23]. On the other hand, we also found that the internal oxidation method not only enhances high-field $J_{c,non\text{-}Cu}$, but at the same time also reduces the low-field $J_{c,non\text{-}Cu}$ due to the point pinning behavior [23]. Conventional Nb_3Sn conductors rely on grain boundary pinning, and the F_p-B curves peak at 20% of the irreversibility fields (B_{irr}). In comparison, the F_p-B curves peak at 1/3 of B_{irr} for point pinning [24]. Since APC conductors have both grain boundary pinning and point pinning, their F_p-B curve peaks shift to higher fields (the extent depending on the fractions of the two components [25]), leading to flattened J_c-B curves. These previous studies using low-field magnetometers (with fields below 9 or 14 T) showed that it is promising to reduce low-field M using the APC approach; however, a full understanding of the F_p-B and J_c-B curves of APC conductors requires a measurement in the whole field range. In this work we measured the J_c-B curves of a reference sample (an RRP® strand) and APC strands using a high-field vibrating sample magnetometer (VSM) up to 27 T. The driving question for this study is, quantitatively, how much can the APC approach reduce the low-field M?

2. Experimental

2.1. Samples

Three samples were measured using the high-field VSM, including a reference sample (an RRP® strand for the HL-LHC) and two APC strands. The RRP® strand has a diameter of 0.85 mm, with 108 Nb_3Sn subelements, and a Cu/non-Cu ratio of ~1.2. The recommended heat treatment of 210°C/48h + 400°C/48h + 665°C/75h with a ramp rate of 25°C/h was used. For the APC strands, our previous studies showed that the Nb alloy (e.g., Nb-Ta-Zr versus Nb-Ta-Hf) – with sufficient oxygen provided – influences the F_p-B curve peak shift [22]. Thus, two APC strands, fabricated using Nb alloy tubes with nominal compositions of Nb-4at.%Ta-1at.%Zr and Nb-4at.%Ta-1at.%Hf, respectively, were studied for this work. Here they are denoted "APC-Zr" and "APC-Hf", respectively. They were fabricated at Hyper Tech Research Inc. based on the PIT filament design using mixtures of Sn, Cu, and SnO_2 powders. Both had 48 Nb_3Sn filaments, with a Cu/non-Cu ratio of 1.15-1.2. They were drawn to 0.72 mm diameter without any breakage. Straight segments were heat treated under vacuum, with the temperature ramped directly to 700°C with a rate of 50°C/h, and then kept at 700°C for 62 hours for both strands. Scanning electron microscopy (SEM) images of the samples after heat treatments are shown in Figure 1.

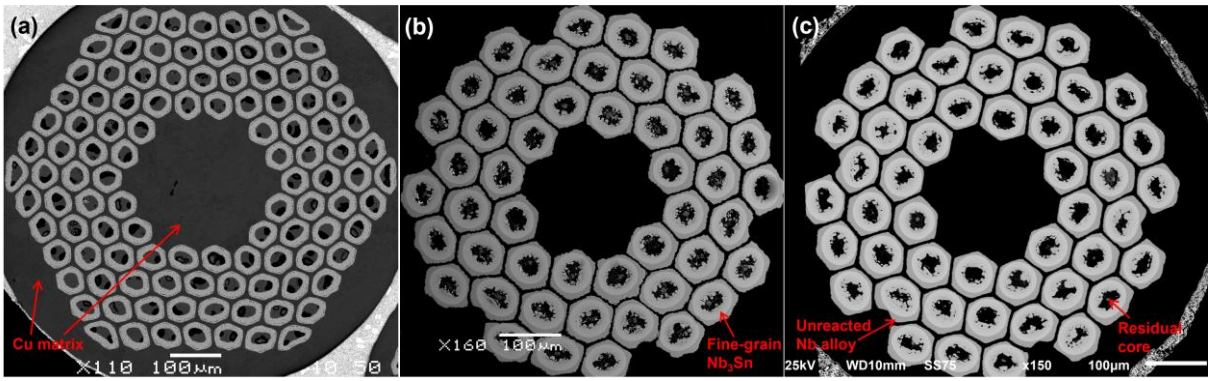

Figure 1. SEM images of (a) the RRP® strand, (b) APC-Zr-700°C/62h, (c) APC-Hf-700°C/62h.

2.2. Measurements

The magnetization versus magnetic field (M-$\mu_0 H$) loops of the samples were measured at 4.2 K up to 27 T (with a ramp rate of 5 T/min) using a VSM installed in a resistive DC magnet at the National High Magnetic Field Laboratory (NHMFL). Straight samples (about 4 mm in length) were measured with the magnetic field perpendicular to the strand length. For each sample great care was taken to ensure that it was within the uniform-field region in the magnet and in the uniform zone of the VSM pickup coil. During the field sweep in some measurements, a change of the sensitivity of the VSM controller caused a spike in the measured M-$\mu_0 H$ loop. The spike regions were trimmed off during data analysis (so there might be gaps in the calculated M-$\mu_0 H$ loops and J_c-B curves), but this does not influence the overall J_c-B results.

3. Results

The measured M-$\mu_0 H$ loops of the samples are shown in Figure 2, with the magnetizations normalized to the non-Cu volumes of the samples. It is seen that the non-Cu $\mu_0 \Delta M$(1 T) of the RRP® strand is about 600 mT, corresponding to ~270 mT normalized to the whole-strand volume (the whole-strand M equals to the non-Cu M multiplied by the non-Cu fraction), nearly two times larger than the $\mu_0 \Delta M$(1 T) requirement given in [4], even though the $J_{c,non\text{-}Cu}$ of this RRP® strand is still significantly below the above-mentioned 16 T $J_{c,non\text{-}Cu}$ specification (to be shown later). The $\mu_0 \Delta M$(1 T) values (normalized to the whole-strand volume) of the APC-Zr and APC-Hf are ~230 and ~190 mT, respectively. Given that their d_{sub} values are ~71 μm, in order to reach the requirement of whole-strand $\mu_0 \Delta M$(1 T) ≤ 150 mT, the d_{sub} values of the APC-Zr and APC-Hf need to be reduced to 46 μm and 56 μm, respectively. Both APC strands have reached or surpassed the 16 T $J_{c,non\text{-}Cu}$ specification (to be shown later). All of the samples showed some

flux jumps below 1 T. For the two APC strands the flux jumps are partially due to the low residual resistivity ratio (RRR) of the Cu matrix. The measured RRR values were 188, 27, and 62 for the RRP®, APC-Zr, APC-Hf samples, respectively. The two APC strands both have very aggressive recipe design, leading to some Sn diffusing into the Cu matrix after the 700°C/62h heat treatment [26]. In [26] we showed that there is still room to optimize the strand design and heat treatment of the current APC strands in order to improve their stability (and thus suppress the flux jumps) without sacrificing their high-field J_c.

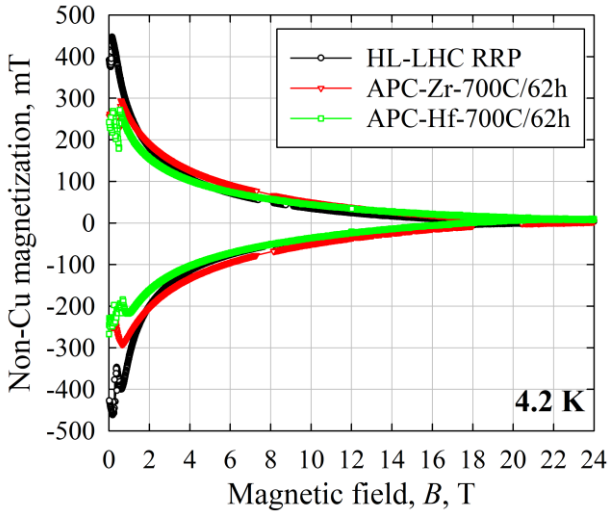

Figure 2. The M-$\mu_0 H$ loops of the samples. The magnetizations are normalized to the non-Cu volumes. Note that the d_{sub} for the RRP® strand is 55 μm, while those of the APC strands are around 71 μm.

The d_{eff} values of the samples were calculated using $d_{eff} = (d_o^3 - d_i^3)/(d_o^2 - d_i^2)$, where d_o and d_i are the outer and inner diameters of the fine-grain Nb_3Sn layers in the subelements, respectively [27]. The calculated d_{eff} values are 69, 79, 77 μm for the RRP®, APC-Zr, and APC-Hf strands, respectively. The $J_{c,non\text{-}Cu}$-B curves of the samples were then calculated using $J_c = 3\pi * \Delta M/(4 d_{eff})$

[27]. A comparison of the magnetic $J_{c,non\text{-}Cu}$ (measured in this work) and the transport values (measured in [23], which used a criterion of 0.1 μV/cm to determine the critical currents) for the RRP® strand is shown in Figure 3.

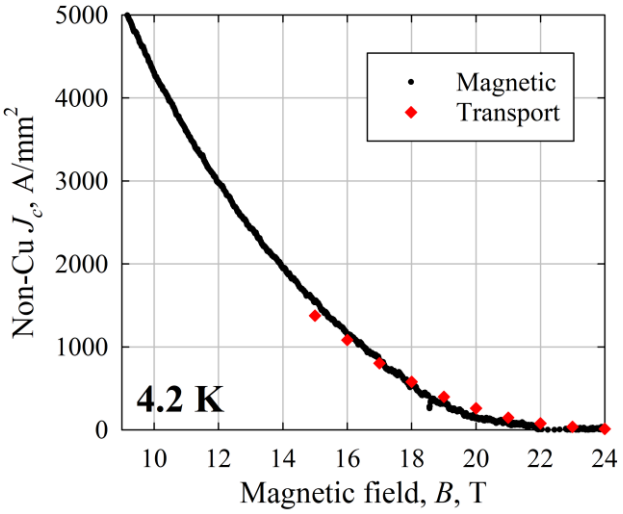

Figure 3. A comparison of the magnetic $J_{c,non\text{-}Cu}$-B curve (measured in this work) and the transport $J_{c,non\text{-}Cu}$ values (measured in [23]) for the RRP® strand.

It is seen that the magnetic and transport $J_{c,non\text{-}Cu}$ values are more or less on the same level. However, the B_{irr}(4.2 K) extracted from the magnetic J_c-B curve is about 21.8 T, while that from the transport result is about 24 T. A previous high-field M-$\mu_0 H$ loop measurement at 4.2 K by Tarantini et al. [28] reported a B_{irr}(4.2 K) of ~22 T for a similar RRP® strand. That study also pointed out the discrepancy between magnetic and transport B_{irr} values. The cause of the discrepancy is still not fully understood yet – we think that it may be partially related to the B_{irr} inhomogeneity (which is due to the Sn content gradient [29]) within the Nb_3Sn layer, but there may be other factors. On the other hand, given that in this study the comparison of the reference

sample and the APC samples is only based on the magnetic measurements, this discrepancy between magnetic and transport B_{irr} values does not influence this comparison.

Figure 4 shows the magnetic $J_{c,non\text{-}Cu}$-B curves of the samples, with the insert figure showing the high-field region. The B_{irr}(4.2 K) values obtained from Figure 4 are 21.8 T, 23.3 T, 22.5 T for the RRP®, APC-Zr, and APC-Hf, respectively. Previous transport measurements – both J_c-B curves and resistivity versus field (R-B) curves – showed that the B_{irr}(4.2 K) values of APC strands are 1.5-2 T higher than that of the RRP® strand [30,31]. Here the magnetic measurements also show higher B_{irr} in the APC strands, but the difference between the APC strands and the RRP® is not as large as that obtained in the transport measurements. It can also be seen from Figure 4 that the J_c-B curves of the APC strands are much flatter than that of the RRP®. The $J_{c,non\text{-}Cu}$-B curves of the APC strands intersect with that of the RRP® at 5 T and 8.7 T for the APC-Zr and APC-Hf, respectively. We can refer to such a field as a "cross-over" field, $B_{cross\text{-}over}$. An APC strand has lower $J_{c,non\text{-}Cu}$ than RRP® below their $B_{cross\text{-}over}$, but has higher $J_{c,non\text{-}Cu}$ above $B_{cross\text{-}over}$. To make the comparison more quantitative, the ratios of the $J_{c,non\text{-}Cu}$ values of the APC strands to those of the RRP® at various fields are listed in Table 1. It can be seen that the higher the field is, the more advantage APC strands have.

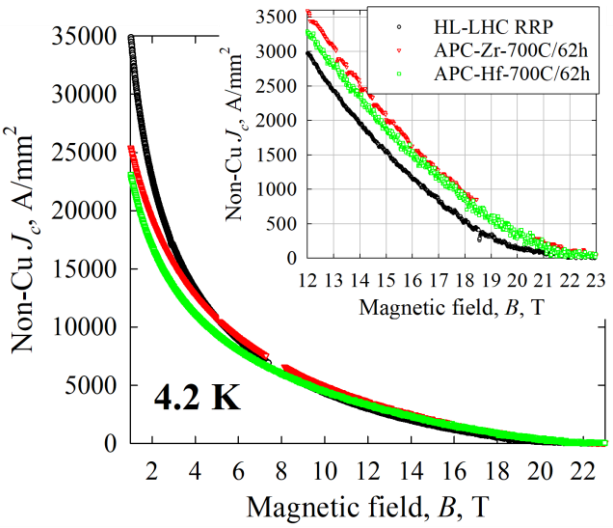

Figure 4. The magnetic $J_{c,non\text{-}Cu}$-B curves of the samples. The insert figure is a blow-up of the high-field region.

Table 1. The ratios of the $J_{c,non\text{-}Cu}$ values of the APC strands to those of the RRP® at various fields.

Ratios of $J_{c,non\text{-}Cu}$ values	1 T	6 T	12 T	16 T	18 T
APC-Zr relative to the RRP®	0.720	1.03	1.20	1.41	1.72
APC-Hf relative to the RRP®	0.655	0.90	1.10	1.32	1.67

In order to understand the relative flatness of the J_c-B curves of the APC strands, the non-Cu F_p (here denoted $F_{p,non\text{-}Cu}$) and the Nb_3Sn layer F_p (here denoted $F_{p,layer}$) versus field curves of the samples were calculated and are shown in Figure 5 (a) and (b), respectively. The $F_{p,layer}$ equals to the $F_{p,non\text{-}Cu}$ divided by the fine-grain Nb_3Sn fractions in the subelements, which are about 59%, 41%, and 39% for the RRP®, APC-Zr, and APC-Hf, respectively. It is seen from Figure 5(a) that the non-Cu maximum pinning force ($F_{p,max}$) values of the two APC strands are quite close to that of the RRP® (with a difference below 10%). Thus, the significant $J_{c,non\text{-}Cu}$ difference between the

APC strands and the RRP® is not due to their difference in non-Cu $F_{p,max}$, but due to the shift in the F_p-B curve peaks of the APC strands. The peak fields (B_p) of the F_p-B curves are 4.9, 6.7, and 7 T for the RRP®, APC-Zr, and APC-Hf, respectively, corresponding to $0.22B_{irr}$, $0.29B_{irr}$, $0.31B_{irr}$, respectively. The F_p-B curve peak shift in the APC strands also accounts for the intersection of their $F_{p,non\text{-}Cu}$-B curves (and $J_{c,non\text{-}Cu}$-B curves in Figure 4) with those of the RRP®. Here it is worth mentioning that the $B_{cross\text{-}over}$ depends not only on the extent of F_p-B curve peak shift, but also on the non-Cu $F_{p,max}$. For example, the $B_{cross\text{-}over}$ of APC-Hf is noticeably higher than that of APC-Zr (8.7 T vs 5 T) mainly because the non-Cu $F_{p,max}$ of APC-Hf is ~12% lower than that of APC-Zr.

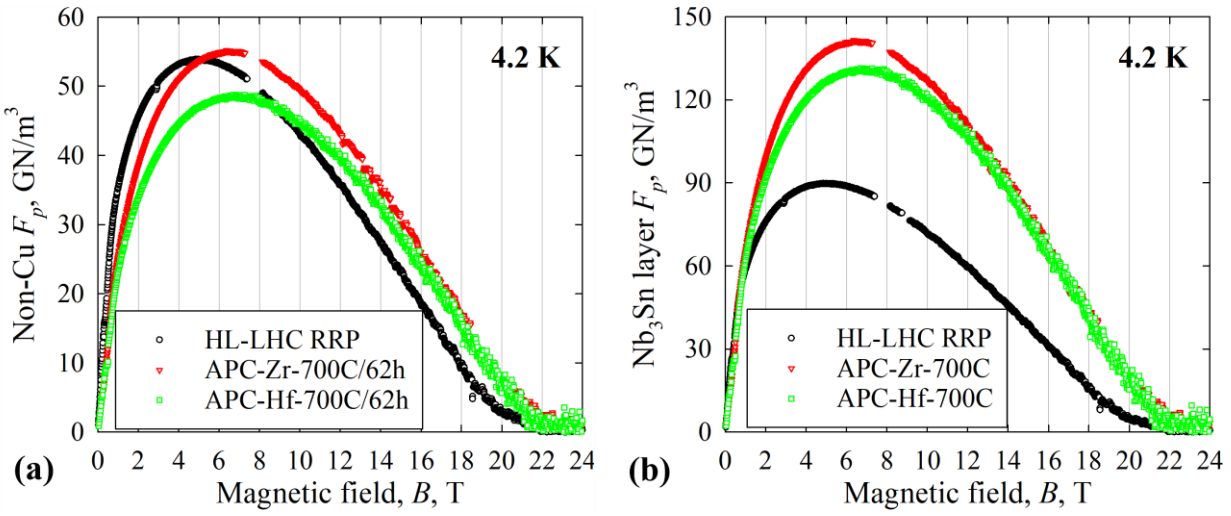

Figure 5. The (a) $F_{p,non\text{-}Cu}$-B and (b) $F_{p,layer}$-B curves of the samples.

4. Discussion

It is easy to understand the increased $J_{c,non\text{-}Cu}$ at high fields for APC Nb_3Sn, but what causes the decrease of $J_{c,non\text{-}Cu}$ at low fields? From Figure 5(b) we see that the $F_{p,layer}$ of the APC strands is mostly higher than that of the RRP®, but this is field dependent – the higher the field is, the

more advantage the APC conductors have, perhaps because the oxide particles work more efficiently at higher fields as flux pinning centers (e.g., due to particle distance matching the flux line spacing better at high fields). On the other hand, the fine-grain Nb_3Sn fractions in the subelements of APC conductors are only about 2/3 of that of the RRP®. At high fields the $F_{p,layer}$ of APC conductors is much higher than that of the RRP® (e.g., it is more than doubled at 16 T) so it dominates over the decrease in Nb_3Sn fraction, but at low fields the increase in $F_{p,layer}$ for APC conductors is not sufficient to compensate the decrease in Nb_3Sn fraction, so a lower $F_{p,non\text{-}Cu}$ is seen at low fields. This causes a cross-over between their $F_{p,non\text{-}Cu}$-B curves.

From Figure 5(b) we also see that APC-Zr has higher layer $F_{p,max}$ than APC-Hf although APC-Hf has more dramatic F_p-B curve peak shift. This is perhaps because, as suggested in our previous paper [26], the HfO_2 particle diameters (mostly 1-5 nm) are smaller than the diameter of the fluxon cores in Nb_3Sn at 4.2 K (~7 nm), which is closer to the ZrO_2 particle diameters (mostly 5-10 nm). However, a comprehensive model taking particle size and distribution as well as grain size into consideration is still needed to compare the APC-Zr and APC-Hf flux pinning characteristics. Besides the alloying element, another factor that influences the F_p-B curve peak shift is the heat treatment temperature. Our previous studies [22] showed that lower heat treatment temperature leads to more dramatic F_p-B curve peak shift and thus flatter J_c-B curve, which is perhaps related to the fact that the oxide particles become smaller as the heat treatment temperature decreases, leading to higher particle volume density and smaller particle distance.

Returning to the driving question of this study – how much can the APC approach reduce the low-field M, an interesting question is, if, by some means, the high-field $J_{c,non\text{-}Cu}$ of conventional Nb_3Sn (i.e., that relies on grain boundary pinning) is increased to the above-mentioned 16 T $J_{c,non\text{-}Cu}$ specification, how is its low-field $J_{c,non\text{-}Cu}$ compared to that of APC Nb_3Sn? In order to

answer this question, let us define a parameter J_c(1 T)/J_c(16 T). If two conductors reach the same required $J_{c,non\text{-}Cu}$ at 16 T, the one with lower J_c(1 T)/J_c(16 T) ratio would have lower $J_{c,non\text{-}Cu}$ (and thus lower M for the same d_{eff}) at 1 T. Based on Figure 4, the calculated J_c(1 T)/J_c(16 T) ratios are 30.9, 15.7, and 15.3 for the RRP®, APC-Zr, APC-Hf strands, respectively. The J_c(1 T)/J_c(16 T) ratios for the APC-Zr and APC-Hf strands reacted at 700°C are quite similar, and are only half of that of the RRP®. In addition, lower heat treatment temperatures are expected to lead to even lower J_c(1 T)/J_c(16 T) ratios as a result of the more dramatic F_p-B curve peak shift and flatter J_c-B curves. It is worth mentioning that the J_c(1 T)/J_c(16 T) ratio is also influenced by the B_{irr}, with a higher B_{irr} leading to a smaller ratio, but the influence of B_{irr} is much less than that of the F_p-B curve peak shift. For example, APC-Hf has slightly lower J_c(1 T)/J_c(16 T) ratio than that of APC-Zr due to the more F_p-B curve peak shift, in spite that it has lower B_{irr} than APC-Zr. In order for the readers to compare the samples more easily, some important parameters are summarized in Table 2. Overall, we see from the above discussions that if both APC and RRP® conductors reach the same $J_{c,non\text{-}Cu}$ at 16 T, the $\mu_0\Delta M$(1 T) of the APC conductors is only half (if reacted at 700°C) or even less (if reacted at lower temperatures) compared with that of the RRP® conductor, assuming they have the same d_{eff}.

Table 2. Some important parameters of the samples for this study.

	B_{irr}(4.2 K), T	B_p, T	$B_{cross\text{-}over}$, T	$J_{c,non\text{-}Cu}$(16 T), A/mm^2	J_c(1 T)/J_c(16 T)
RRP®	21.8	4.9	-	1150	30.9
APC-Zr	23.3	6.7	5	1620	15.7
APC-Hf	22.5	7	8.7	1520	15.3

5. Conclusions

With the required much higher $J_{c,non\text{-}Cu}$ for Nb_3Sn conductors for the high-field accelerator magnet application, the low-field magnetization becomes a critical challenge because it leads to low-field instability (e.g., flux jumps), AC loss, and field errors in the magnet bores. Reduction of d_{eff} is effective in suppressing magnetization, but a significant reduction of d_{eff} without sacrificing the high-field $J_{c,non\text{-}Cu}$ is difficult to realize technically. An alternative approach to reducing the low-field magnetization is using the internal oxidation method, which forms oxide particles (mostly 1-10 nm) that serve as point pinning centers and cause the F_p-B curve peak to shift to higher fields. To quantitatively study how much the APC approach can reduce the low-field magnetization, in this work we measured a reference sample (an RRP® strand for HL-LHC) and two APC strands (based on internal oxidation of Nb-Ta-Zr and Nb-Ta-Hf, respectively) reacted at 700°C using a VSM up to 27 T. The results showed that the F_p-B curve peak shift in the APC strands leads to much flatter J_c-B curves relative to conventional Nb_3Sn (i.e., those relying on grain boundary pinning). The $F_{p,non\text{-}Cu}$-B curves of the APC strands intersect with that of RRP® at 5-9 T; the APC strands have higher $J_{c,non\text{-}Cu}$ above the cross-over fields (e.g., 32-41% higher at 16 T), but have lower $J_{c,non\text{-}Cu}$ below the cross-over fields (e.g., around 30% lower at 1 T). This is because the enhancement of Nb_3Sn layer F_p and J_c via the internal oxidation method is weak at low fields and becomes more significant with the increase of the field; on the other hand, the fine-grain Nb_3Sn fractions in subelements of the APC conductors are only 2/3 of that in the RRP® conductor. It is the combination of these two effects that causes a cross-over between the $J_{c,non\text{-}Cu}$-B curves of an RRP® and an APC conductor. By comparing the parameter J_c(1 T)/J_c(16 T), we see that if APC and RRP® conductors reach the same $J_{c,non\text{-}Cu}$ at 16 T, the $J_{c,non\text{-}Cu}$ and thus magnetization (for the same d_{eff}) at 1 T of APC strands are only half (if reacted at 700°C) or even less (if reacted at lower temperatures) relative to those of RRP®. As a result, to

achieve the same magnetization at 1 T – e.g., the goal of $\mu_0\Delta M(1\text{ T}) \leq 150$ mT proposed in [4], APC strands can have twice as large d_{eff} as RRP® (e.g., 40 μm instead of 20 μm). This is a significant advantage of APC conductors with respect to RRP®, because a d_{eff} of 40 μm is achievable (for the PIT design) but a d_{eff} of 20 μm is hardly achievable if we want to retain high $J_{c,non\text{-}Cu}$ at high fields.

Acknowledgements

This work was supported by the US Department of Energy through an Early Career Research Program Award and Hyper Tech SBIR DE-SC0017755. A portion of this work was performed in the NHMFL, which is supported by National Science Foundation Cooperative Agreement No. DMR-1644779 and the State of Florida. This manuscript has been produced by Fermi Research Alliance, LLC under Contract No. DE-AC02-07CH11359 with the U.S. Department of Energy, Office of Science, Office of High Energy Physics.

References

[1]. Abada A *et al.* 2019 FCC-hh: the hadron collider *Eur. Phys. J. Special Topics* **228** 755–1107
[2]. Bottura L *et al.* 2022 A work proposal for a collaborative study of magnet technology for a future muon collider arXiv:2203.13998 [physics.acc-ph]
[3]. Rochepault E, Ferracin P and Vallone G 2022 20 T Hybrid Nb_3Sn-HTS block-coil designs for a future particle collider *IEEE Trans. Appl. Supercond.* **32** 4003505
[4]. Ballarino A and Bottura L 2015 Targets for R&D on Nb_3Sn conductor for high energy physics *IEEE Trans. Appl. Supercond.* **25** 6000906
[5]. Tommasini D and Toral F 2016 Overview of magnet design options *EuroCirCol-P1-WP5 report* 4-6
[6]. Wilson M N 1983 Superconducting magnets, Clarendon Press, Oxford
[7]. Collings E W, Sumption M D and Lee E 2001 Magnetization as a critical defining parameter for strand in precision dipole applications-implications for field error and F-J stability *IEEE Trans. Appl. Supercond.* **11** 2567–70

[8]. Xu X, Sumption M D and Collings E W 2014 Influence of heat treatment temperature and Ti doping on low field flux jumping and stability in (Nb-Ta)$_3$Sn strands *Supercond. Sci. Technol.* **27** 095009
[9]. Izquierdo Bermudez S, Tommasini D and Bordini B 2017 AC loss for EuroCirCol 16 T designs https://indico.cern.ch/event/679654/contributions/2783604/attachments/1553893/2442764/171102_FCC_ACloss.pdf
[10]. Wang X *et al*. 2015 Validation of Finite-Element Models of Persistent-Current Effects in Nb_3Sn Accelerator Magnets *IEEE Trans. Appl. Supercond.* **25** 4003006
[11]. Izquierdo Bermudez S, Bottura L and Todesco E 2016 Persistent-Current Magnetization Effects in High-Field Superconducting Accelerator Magnets *IEEE Trans. Appl. Supercond.* **26** 4003905
[12]. Ghosh A K, Cooley L D, Moodenbaugh A R, Parrell J A, Field M B, Zhang Y and Hong S 2005 Magnetization studies of high J_c Nb_3Sn strands *IEEE Trans. Appl. Supercond.* **15** 3494-7
[13]. Parrell J A, Zhang Y, Field M B and Hong S 2007 Development of internal tin Nb_3Sn conductor for fusion and particle accelerator applications *IEEE Trans. Appl. Supercond.* **17** 2560-3
[14]. Bordini B, Richter D, Alknes P, Ballarino A, Bottura L and Oberli L 2013 Magnetization measurements of high-J_c Nb_3Sn strands *IEEE Trans. Appl. Supercond.* **23** 7100806
[15]. Field M B, Zhang Y, Miao H, Gerace M, and Parrell J A 2014 Optimizing Nb_3Sn conductors for high field applications *IEEE Trans. Appl. Supercond.* **24** 6001105
[16]. Sanabria C 2017 A new understanding of the heat treatment of Nb-Sn superconducting strands *PhD dissertation* Florida State University
[17]. Lindenhovius J L H, Hornsveld E M, den Ouden A, Wessel W A J and ten Kate H H J 2000 Powder-in-Tube (PIT) Nb_3Sn conductors for high-field magnets *IEEE Trans. Appl. Supercond.* **10** 975-8
[18]. Godeke A, Den Ouden A, Nijhuis A and ten Kate H H J 2008 State of the art powder-in-tube niobium–tin superconductors *Cryogenics* **48** 308-16
[19]. Peng X *et al* 2011 Strain and magnetization properties of high subelement count tube-type Nb_3Sn strands *IEEE Trans. Appl. Supercond.* **21** 2559-62
[20]. Xu X, Sumption M D, Peng X and Collings E W 2014 Refinement of Nb_3Sn grain size by the generation of ZrO_2 precipitates in Nb_3Sn strands *Appl. Phys. Lett.* **104** 082602
[21]. Xu X, Sumption M D and Peng X 2015 Internally oxidized Nb_3Sn superconductor with very fine grain size and high critical current density *Adv. Mater.* **27** 1346-50
[22]. Xu X, Peng X, Rochester J, Sumption M D, Lee J, Ortiz G A C and Hwang J 2021 The strong influence of Ti, Zr, Hf solutes and their oxidation on microstructure and performance of Nb_3Sn superconductors *J. Alloys Compd.* **857** 158270
[23]. Xu X, Peng X, Lee J, Rochester J and Sumption M D 2020 High critical current density in internally-oxidized Nb_3Sn superconductors and its origin *Scr. Mater.* **186** 317-320
[24]. Hughes D 1974 Flux pinning mechanisms in type II superconductors *Phil. Mag.* **30** 293-305
[25]. Rochester J, Ortino M, Xu X, Peng X and Sumption M 2021 The roles of grain boundary refinement and nano-precipitates in flux pinning of APC Nb_3Sn *IEEE Trans. Appl. Supercond.* **31** 8000205

[26]. Xu X, Peng X, Wan F, Rochester J, Bradford G, Jaroszynski J and Sumption M 2023 APC Nb_3Sn superconductors based on internal oxidation of Nb-Ta-Hf alloys *Supercond. Sci. Technol.* **36** 035012
[27]. Sumption M D, Peng X, Lee E, Wu X and Collings E W 2004 Analysis of magnetization, ac loss, and d_{eff} for various internal-Sn based Nb_3Sn multifilamentary strands with and without subelement splitting *Cryogenics* **44** 711–25
[28]. Tarantini C, Balachandran S, Heald S M, Lee P J, Paudel N, Choi E S, Starch W L and Larbalestier D C 2019 Ta, Ti and Hf effects on Nb_3Sn high-field performance: temperature-dependent dopant occupancy and failure of Kramer extrapolation *Supercond. Sci. Technol.* **32** 124003
[29]. Baumgartner T, Pfeiffer S, Bernardi J, Ballarino A and Eisterer M 2018 Effects of inhomogeneities on pinning force scaling in Nb_3Sn strands *Supercond. Sci. Technol.* **31** 084002
[30]. Xu X, Sumption M D, Lee J, Rochester J and Peng X 2020 Persistent compositions of non-stoichiometric compounds with low bulk diffusivity: a theory and application to Nb_3Sn superconductors *J. Alloys Compd.* **845** 156182
[31]. Buta F *et al* 2021 Very high upper critical fields and enhanced critical current densities in Nb_3Sn superconductors based on Nb–Ta–Zr alloys and internal oxidation *J. Phys. Mater.* **4** 025003